Table of Contents

Extended Mathematical model:

To gain insight into the feed-forward mechanism governing Far1 activity, we developed an ODE model for the concentration of active and inactive Far1:

$$\frac{dFar1^{active}}{dt} = f_1[\alpha(t)]Far1^{inactive} - Far1^{active}\left(k_3 + k_2(t)\right) \text{ (Eq. 1)}$$

$$\frac{dFar1^{inactive}}{dt} = f_0[\alpha(t)] + k_3 Far1^{active} - Far1^{inactive}\left(f_1[\alpha(t)] + k_2(t)\right) \text{ (Eq. 2)}$$

$$\frac{dFar1^{total}}{dt} = f_0[\alpha(t)] - k_2(t)Far1^{total} \text{ (Eq. 3)}$$

$$Far1^{total} = Far1^{active} + Far1^{inactive} \text{ (Eq. 4)}$$

Here $f_0[\alpha(t)]$, $f_1[\alpha(t)]$, $k_2(t)$, and k_3 denote the Far1 production, phosphorylation, degradation or dilution and dephosphorylation rates respectively. Time-dependent degradation and dilution is due to cell growth or CDK-mediated degradation. Additionally, the synthesis rate $f_0[\alpha(t)]$ is time-dependent and also likely reflects cell growth. $\alpha(t)$ represents α-factor-induced Fus3 activity. We note that the total amount of Far1 equals the sum of the active and inactive Far1 (Eq. 4), which allows us to rewrite the equations as follows:

$$\frac{dFar1^{active}}{dt} = f_1[\alpha(t)]Far1^{total} - Far1^{active}(f_1[\alpha(t)] + k_2(t) + k_3) \text{ (Eq. 5)}$$

$$\frac{dFar1^{total}}{dt} = f_0[\alpha(t)] - k_2(t)Far1^{total} \text{ (Eq. 6)}$$

Next, we rearrange the terms of (Eq.6) and multiply both sides with the integrating factor $e^{\int_0^t k_2(t')dt'}$

$$\frac{d}{dt}\left(e^{\int_0^t k_2(t')dt'} Far1^{total}\right) = f_0[\alpha(t)]e^{\int_0^t k_2(t')dt'} \text{ (Eq. 7)}$$

Next, we integrate from $\mathbf{0}$ to time $T>0$ and specify the initial condition $Far1^{total}(\mathbf{0}) = F_0$:

$$\int_0^T \frac{d}{dt}\left(e^{\int_0^t k_2(t')dt'} Far1^{total}\right)dt = \int_0^T f_0[\alpha(t)]e^{\int_0^t k_2(t')dt'}\, dt \text{ (Eq. 8)}$$

which yields

$$Far1^{total}(T) = \int_0^T f_0[\alpha(t)]e^{-\int_t^T k_2(t')dt'}\, dt + F_0 e^{-\int_o^T k_2(t)dt'} \text{ (Eq. 9)}$$

The total amount of Far1 therefore depends on the pathway history with a memory decay factor that depends on the history of the degradation or dilution rate $k_2(t)$. Next, we combine Eq. 9 with Eq.5 and multiply with the integrating factor $e^{\int_0^t (f_1[\alpha(\tau)]+k_2(\tau)+k_3)d\tau}$:

$$\frac{d}{dt}\left(Far1^{active} e^{\int_0^t (f_1[\alpha(\tau)]+k_2(\tau)+k_3)d\tau}\right) = f_1[\alpha(t)]Far1^{total} e^{\int_0^t (f_1[\alpha(\tau)]+k_2(\tau)+k_3)d\tau} \text{ (Eq.10)}$$

which can be integrated:

$$\int_0^T \frac{d}{dt}\left(\boldsymbol{Far1^{active}} e^{\int_0^t (f_1[\alpha(\tau)]+k_2(\tau)+k_3)d\tau}\right)\boldsymbol{dt} = \int_0^T \boldsymbol{f_1[\alpha(t)]Far1^{total}} e^{\int_0^t (f_1[\alpha(\tau)]+k_2(\tau)+k_3)d\tau}\boldsymbol{dt}$$
(Eq.11)

so that

$$\boldsymbol{Far1^{active}(T)} = \int_0^T \boldsymbol{f_1[\alpha(t)]Far1^{total}(t)} e^{-\int_t^T (f_1[\alpha(\tau)]+k_2+k_3)d\tau}\,\boldsymbol{dt}$$ (Eq. 12)

Note that we used the initial condition $\boldsymbol{Far1^{active}(0) = 0}$. Typically, phosphorylation and dephosphorylation rates are faster than changes in protein concentration (production, dilution and degradation rates) that is: ($f_1[\alpha(t)] >> k_2(t)$, $k_3 >> k_2(t)$, $f_1[\alpha(t)] >> f_0[\alpha(t)]$,$k_3 >> f_0[\alpha(t)]$). We expect that phosphorylation kinetics are equilibrated on a fast time scale. This allows us to rewrite Eq.5 in the following way:

$$\frac{dFar1^{active}}{dt} \approx \boldsymbol{0} \approx \boldsymbol{f_1[\alpha(T)]Far1^{total} - Far1^{active}(f_1[\alpha(T)] + k_3)}$$ (Eq. 13)

Which we can rewrite as:

$$\boldsymbol{Far1^{active}} = \frac{f_1[\alpha(T)]}{f_1[\alpha(T)]+k_3}\boldsymbol{Far1^{total}}$$ (Eq. 14)

We can now combine equations 9 and 14 yielding an approximate expression for active Far1:

$$\boldsymbol{Far1^{active}(T)} = \frac{f_1[\alpha(T)]}{f_1[\alpha(T)]+k_3}\left(\int_0^T \boldsymbol{f_0[\alpha(t)]} e^{-\int_t^T k_2(t')dt'}\,\boldsymbol{dt} + \boldsymbol{F_0} e^{-\int_o^T k_2(t')dt'}\right)$$ (Eq. 15)

The amount of active Far1 thus corresponds to the amount of total Far1 times a factor determined by how large the phosphorylation rate $f_1[\alpha(t)]$ is compared with the sum of the phosphorylation, and dephosphorylation rates ($f_1[\alpha(t)] + k_3$). The amount of active Far1 is thus determined by two timescales: A fast timescale corresponding to the phosphorylation or dephosphorylation equilibrium and a slow timescale which reflects the degradation or dilution rate. For growth rates approximating exponential, $k_2(t) = k_2$, and Eq. 15 simplifies to Eq. 3 in the main text and to the solutions shown in Fig. S5.

Mathematical models for the alternative systems

We here explore alternative network structures that might control mating pathway signaling as depicted in Fig. S5 and S8. We note that we will use the same notations as for the feed-forward model above as far as possible:

Transcription only: Here Far1 is controlled only by transcription (see Fig. S8) so that

$$\frac{dFar1^{active}}{dt} = f_0[\alpha(t)] - k_2(t)Far1^{active} \quad \text{(Eq. 16)}$$

This equation is identical to the expression for the total amount of Far1 in the feed-forward case (eq.6) and has the same solution (eq. 9):

$$Far1^{active}(T) = \int_0^T f_0[\alpha(t)]e^{-\int_t^T k_2(t')dt'}\,dt + F_0 e^{-\int_o^T k_2(t)dt'} \quad \text{(Eq. 17)}$$

where F_0 is the initial amount of Far1, since all Far1 is active here we set $F_0 = 0$ as active Far1 would greatly delay G1 for cycling cells not exposed to mating pheromone. Thus,

$$Far1^{active}(T) = \int_0^T f_0[\alpha(t)]e^{-\int_t^T k_2(t')dt'}\,dt \quad \text{(Eq. 18)}$$

Phosphorylation only: We here assume that there is a constant amount of Far1 which is solely phospho-regulated:

$$\frac{dFar1^{active}}{dt} = Far1^{inactive}f_1[\alpha(t)] - k_3 Far1^{active} \quad \text{(Eq. 19)}$$

$$\frac{dFar1^{inactive}}{dt} = -Far1^{inactive}f_1[\alpha(t)] + k_3 Far1^{active} \quad \text{(Eq. 20)}$$

$$Far1^{total} = Far1^{active} + Far1^{inactive} \quad \text{(Eq. 21)}$$

Combining equations 19 and 21 yields:

$$\frac{dFar1^{active}}{dt} = Far1^{total}f_1[\alpha(t)] - (k_3 + f_1[\alpha(t)])Far1^{active} \quad \text{(Eq. 22)}$$

Which can be solved in the same way as equation 6 by substituting $f_0[\alpha(t)]$ with $Far1^{total}f_1[\alpha(t)]$ and $k_2(t)$ with $k_3+f_1[\alpha(t)]$. This gives us the following solution:

$$\boldsymbol{Far1^{active}(T) = Far1^{total} \int_0^T f_1[\alpha(t)] e^{-\int_t^T (k_3 + f_1[\alpha(t')])dt'} \, dt}$$ (Eq. 23)

To assure that cells can cycle when the MAPK pathway is off we have assumed that $Far1^{active}(0)=0$.

Positive feedback: To model a generalized positive feedback case we use the same model as for the feed-forward system (supporting equations 1-4) but now allow the pathway activity to be hysteretic as shown in Fig. S5C, 2nd and 3rd columns. This may arise due to feedback in the MAPK pathway such that Fus3 activity is self-reinforcing through some unspecified mechanism. Thus Fus3 activity ~ $f(\alpha(T < t))$ where the history of exposure to pheromone determines the branch of the multivalued output. Thus, the active Far1 follows the following equation

$$\boldsymbol{\frac{dFar1^{active}}{dt} = k_1 f\big(\alpha(T < t)\big) Far1^{inactive} - Far1^{active}\big(k_3 + k_2(t)\big)}$$ (Eq. 24),

where k_1 is a constant. Thus, equation 24 can be rewritten (using equation 4) as follows:

$$\boldsymbol{\frac{dFar1^{active}}{dt} = k_1 f\big(\alpha(T < t)\big)\big(Far1^{total} - Far1^{active}\big) - Far1^{active}\big(k_3 + k_2(t)\big)}$$ (Eq. 25)

Performance:
To determine the characteristics of the different systems we calculate their performance given four criteria: arrest time, reentry time, noise resistance and the input-output relationship, ability to measure the extracellular environment. Notably, to substantiate our claim in Fig. S8 and the main text we only need to show (i) that feed-forward can fulfill all criteria and (ii) each other network fails to meet at least one criterion. For simplicity we here assume that all rates (summarized in Table S3) are constant unless otherwise stated. The results are shown in Fig. S5.

Motivation for performance criteria:

(i) Rapid arrest allows faster mating which may be beneficial in a competitive environment where the diploid state is advantageous.

(ii) Rapid reentry allows for continued asexual growth in the case of failed mating (competitor mates instead, mating partner dies, etc…).

(iii) Noise resistance is necessary to remain arrested in the presence of fluctuations. Notably, the arrested state is more robust *if and only if* the cell was previously exposed to a high concentration of mating pheromone indicating increased probability of a nearby mating partner. It would therefore be advantageous for a cell once exposed to a high concentration of mating pheromone to stay arrested as a temporary lowering of mating most likely is caused by noise. Importantly this differs from the

case when the cell is outcompeted and has to resume asexual growth (see point (ii) above)

(iv) Maintaining a constant input – output relationship between pheromone concentration and MAPK activity is necessary for accurate information processing which may be crucial for chemotrophism and fusion.

Feed-forward:

Arrest: We here assume that there is some level of active Far1 'y', that a cell needs to reach to arrest. Furthermore as cells arrest almost instantaneously after exposure to mating pheromone we assume that the initial amount of $Far1^{inactive}$ (= F_0), is larger than this level. We can therefore ignore the slower time-scales $f_0[\alpha(t)]$ and k_2 and calculate the time it takes to phosphorylate the initial amount of (inactive) Far1, F_0:

$$\frac{dFar1^{active}}{dt} = -k_3 Far1^{acitve} + f_1[\alpha(t)]F_0 \text{ (eq. 26)}$$

Much like equation 22, this equation can be solved in the same way as equation 6 by substituting $f_0[\alpha(t)]$ with $f1[\alpha(t)]F_0$ and $k_2(t)$ with k_3. Note that we assume that all rates are constant in time on this short time scale including $f_1[\alpha(t)] = k_1\alpha$. This gives us the following solution:

$$Far1^{active}(T) = \int_0^T k_1 \alpha F_0 e^{-\int_t^T k_3 dt'} dt \underset{here}{\Longleftrightarrow} Far1^{active}(T) = \frac{k_1 \alpha F_0}{k_3}(1 - e^{-k_3 T}) \text{ (eq. 27)}$$

We can now calculate the time it takes to reach 'y':

$$t_{arrest} = -\frac{1}{k_3} ln\left(1 - \frac{y k_3}{k_1 \alpha F_0}\right) \underset{exp}{\overset{taylor}{\Longleftrightarrow}} t_{arrest} = \frac{y}{k_1 \alpha F_0} + higher\ order\ terms \text{ (eq. 28)}$$

Notably, the arrest time-scale depends mostly on the (fast) phosphorylation rate which ensures a rapid arrest. This can be seen easily after expanding the logarithm in equation 28.

Reentry: We solve for the case where α = 0, in equations 5 and 6:

$$Far1^{active} = \frac{k_1 \alpha_{st.st.}}{k_1 \alpha_{st.st.} + k_3} \frac{k_0 \alpha_{st.st.}}{k_2} e^{-(k_2 + k_3)t} \text{ (eq. 28)}$$

Note that $\frac{k_1 \alpha_{st.st.}}{k_1 \alpha_{st.st.} + k_3} \frac{k_0 \alpha_{st.st.}}{k_2}$ is the steady state value of $Far1^{active}$ and $k_{0/1}\alpha_{st.st.}$ is the pre-reentry value of $f_{0/1}[\alpha(t)]$ which is assumed to be constant. We can thus solve the time '$t_{reentry}$' it takes to reach the critical level y:

$y = Far1_{st.st.}^{active} e^{-k_3 t}$ (eq. 29)

Thus, the amount of active Far1 reaches the critical level y at the time

$t_{reentry} = -\frac{1}{k_3} ln\left[\frac{y}{Far1_{st.st.}^{active}}\right]$ (eq. 30)

Note we here and elsewhere, we used $k_3 >> k_2$.

Noise resistance:

Our solution indicates that the amount of $Far1^{active}$ will correspond to the phosphorylation rate times the accumulated pathway activity. This implies that the main source of noise resistance in the feed-forward system is the accumulation of Far1. To quantify this value we measured the relative increase of maximal Far1 for cycling cells compared with arrested cells (see Fig. S5H). We found that the average increase was 6.6±2.2 times (N=32), in good agreement with previously reported bulk measurements (Chang and Herskowitz, 1990). Since the peak value for cycling cells is sufficient to induce cell cycle arrest, our results therefore suggests that the feed-forward circuit can handle at least a 6-fold temporary decrease in mating pathway activity.

Transcription only:

Here we assume that all Far1 produced is active and that all regulation is governed by production, degradation and dilution. Assuming that all rates are constant (including $k_0\alpha_{st.st.}$ as in the *reentry* section) we get the following expression from equation 9 for the 'transcription only' case:

$Far1^{active}(t) = \frac{k_0\alpha_{st.st.}}{k_2}(1 - e^{-k_2 t})$ (eq. 31)

As all Far1 is active here we assume that Far1(0) = 0. Using this expression we can calculate the expressions for t_{arrest} and $t_{reentry}$ (using the same assumptions as above):

$t_{arrest} = -\frac{1}{k_2} ln\left[1 - \frac{yk_2}{k_0\alpha_{st.st.}}\right], t_{reentry} = -\frac{1}{k_2} ln\left[\frac{y}{\frac{k_0\alpha_{st.st.}}{k_2}}\right]$ (eq. 32)

Where y represents the level to which we calculate the drop as above. We see that both arrest and reentry scales with the slower degradation/dilution rate which is inconsistent with rapid arrest and reentry. Note that the steady state value in this case equals ($k_0\alpha_{st.st.}/k_2$).

Phosphorylation only:

As a system governed solely by phosphorylation (Fig. S5,8 eqn's 19-23), can arrest and reenter the cell cycle rapidly, we will here argue that it is expected to be less noise resistant than a feed-forward system. Just like the feed-forward case, a phosphorylation only system will respond to changes in pathway activity on a rapid time-scale corresponding to phosphorylation and

dephosphorylation, $f_1[\alpha(t)]$ and k_3. The difference between the two systems is that the total amount of Far1 can be regulated transcriptionally in response to mating pheromone for the feed-forward, but not for the phosphorylation only system. Thus either the phosphorylation system retains a low amount of Far1 which will make it susceptible to pathway fluctuations or the initial amount of Far1 is always very high. This latter alternative is unlikely for two main reasons: (i) It is known that Far1 is substantially upregulated in response to mating pheromone and the initial amount is small compared with the amount in permanently (i.e. high pheromone) arrested cells (ii) Unphosphorylated Far1 retains some residual ability to inhibit G1 cyclins (M.Loog pers. comm., also see (Busti et al., 2012)). A large pool of inactive Far1 would therefore interfere with normal cell cycle progression. Moreover, even in this case the feed-forward system would perform *even* better as it may further up-regulate the total amount of Far1 as desired. We therefore conclude that a phosphorylation only motif is not sufficient to perform adequately.

Positive feedback:

We analyzed numerically a model with bistable MAPK activity (output) in response to mating pheromone (input). Note that it is always possible to tweak the parameters for positive feedback such that bistability disappears. However this also requires that arrest stability has been lost. Thus, positive feedback models cannot both provide stability and maintain a single-valued input-output relationship (Fig. S8D-F, Table S3).

Figure S1, related to Figure 1:

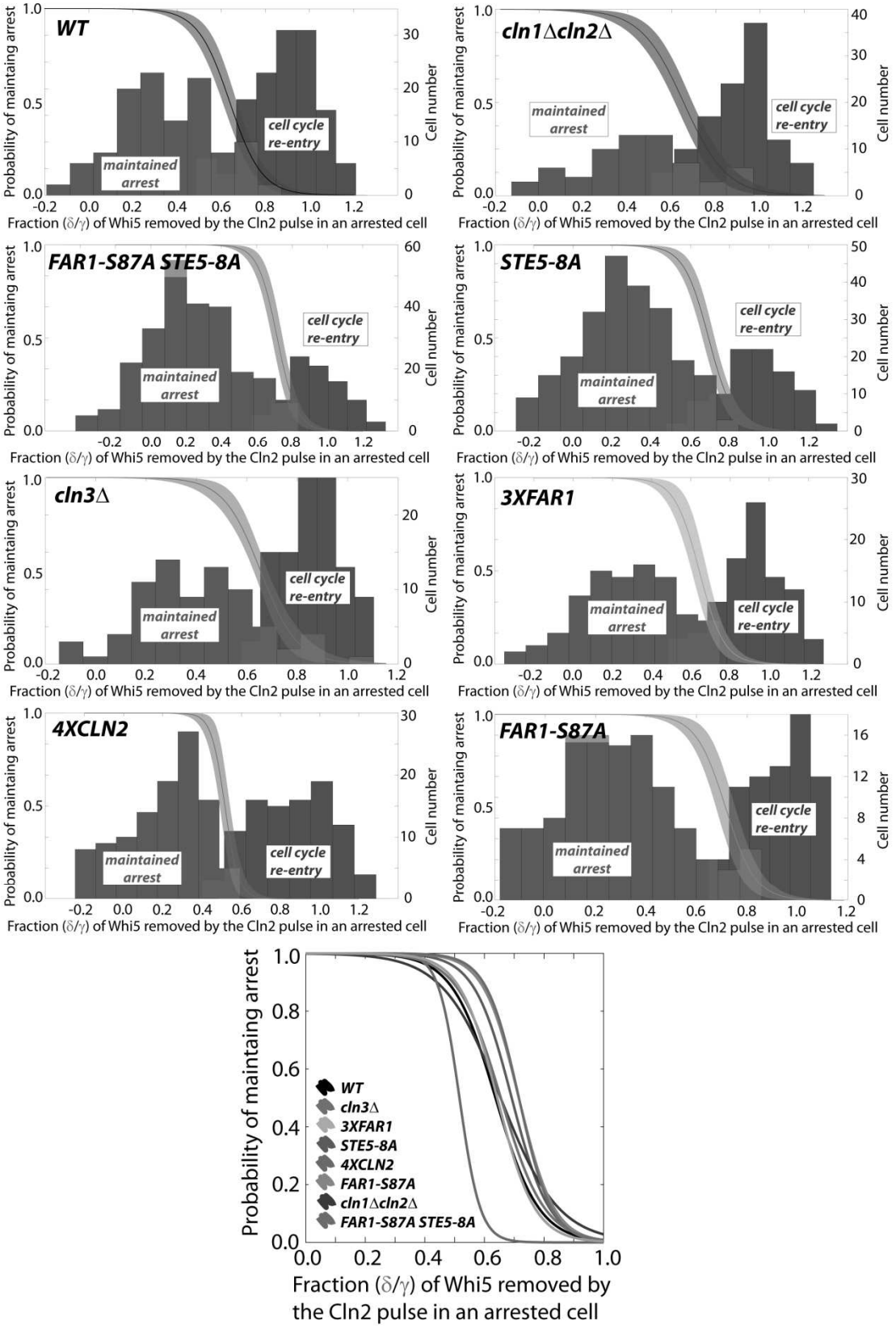

Genetic analysis of exogenously forced cell cycle reentry: Arrested cells of the specified genotype were exposed to a pulse of exogenous Cln2 expressed from a *MET3* promoter as described in Fig. 1B,C. Next, the probability of the two cell fates (cell cycle reentry or maintained arrest) was calculated using logistic regression as previously described (Doncic et al., 2011). We found that the CDK-threshold to reenter the cell cycle from mating arrest is significantly higher for WT, *STE5-8A* and *cln3Δ* cells. Indeed, only the addition of 3 copies of *CLN2* had a large effect on the Whi5 threshold for cell cycle reentry. Neither *FAR1-S87A* nor *STE5-8A* mutated alleles that cannot be inhibited by the G1 cyclins affect the reentry threshold. The reason for this may be that after arrest induced Far1 accumulation, it takes a longer and more sustained pulse of exogenous Cln2 to deplete the accumulated Far1 to the extent that the endogenous cyclin positive feedback loop can function autonomously. Due to the rapid degradation of G1 cyclins, premature withdrawal of the exogenously controlled Cln2 will result in the residual Far1 inhibiting endogenous Cln2 to the extent that all Cln2 synthesis is inactivated and the cell remains arrested. For statistical comparisons see Table S1. N_{WT} =251, $N_{STE5\text{-}8A}$ =325, N_{4xCLN2} = 204, N_{3XFAR1} = 187, $N_{cln3\Delta}$ = 190, $N_{FAR1\text{-}S87A}$ = 185, $N_{cln1\Delta cln2\Delta}$ = 177 and $N_{FAR1\text{-}S87A\ STE5\text{-}8A}$ = 337. Shaded areas represent 95% confidence intervals from 10000 bootstrapping iterations.

Figure S2, related to Figure 2:

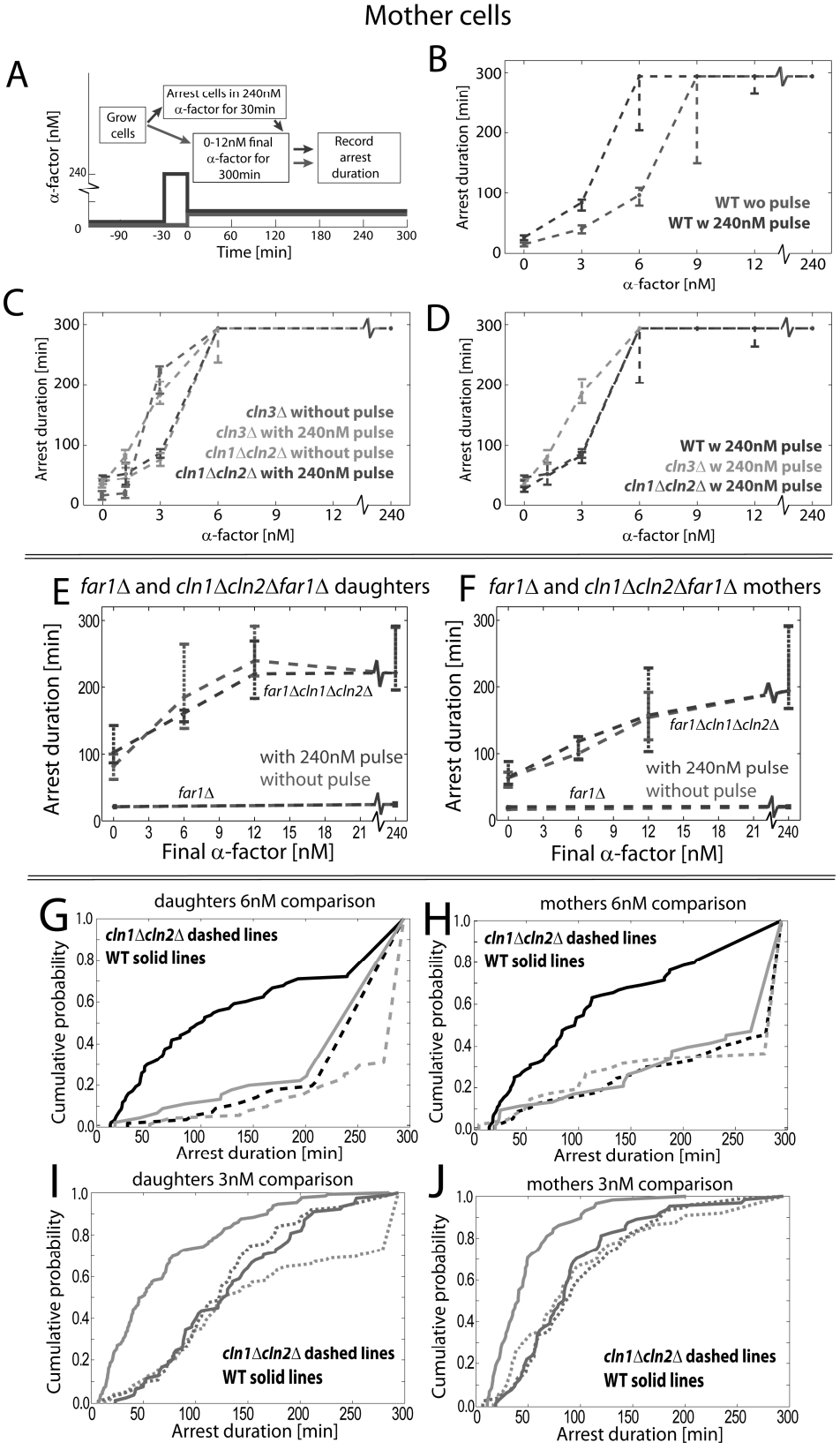

Analysis of hysteresis in cell cycle kinetics for mother cells and mutants: (A-D) Data for daughter cells are shown in the main text. (A) Experiment schematic (see methods). (B) Duration of arrest in mother cells exposed to a 30 min pulse of high mating pheromone concentration or control cells. (C) Lack of hysteresis in cells lacking Cln1 and Cln2. (D) Arrest kinetics in cells experiencing a pheromone pulse lacking either Cln3, or Cln1 and Cln2. (*E-F) Hysteresis depends primarily on Far1-dependent inhibition of Cln1 and Cln2*: Experiments are similar to those presented in Fig. 2A-D. *far1*Δ and *far1*Δ*cln1*Δ*cln2*Δ cells do not exhibit hysteresis. Data in (B-F) are medians with 95% confidence intervals calculated using 10000 bootstrapping iterations. For statistics of the distribution of reentry times see Fig. S3. (G-J) Comparison of the full arrest distributions for individual *WT* and *cln1*Δ*cln2*Δ cells with and without the 240nM pheromone pulse reveals the similarity between *WT* cells which were exposed to the pulse and *cln1*Δ*cln2*Δ cells. Colors indicate mating pheromone exposure history as indicated in Fig. S3.

Figure S3, related to Figure 2:

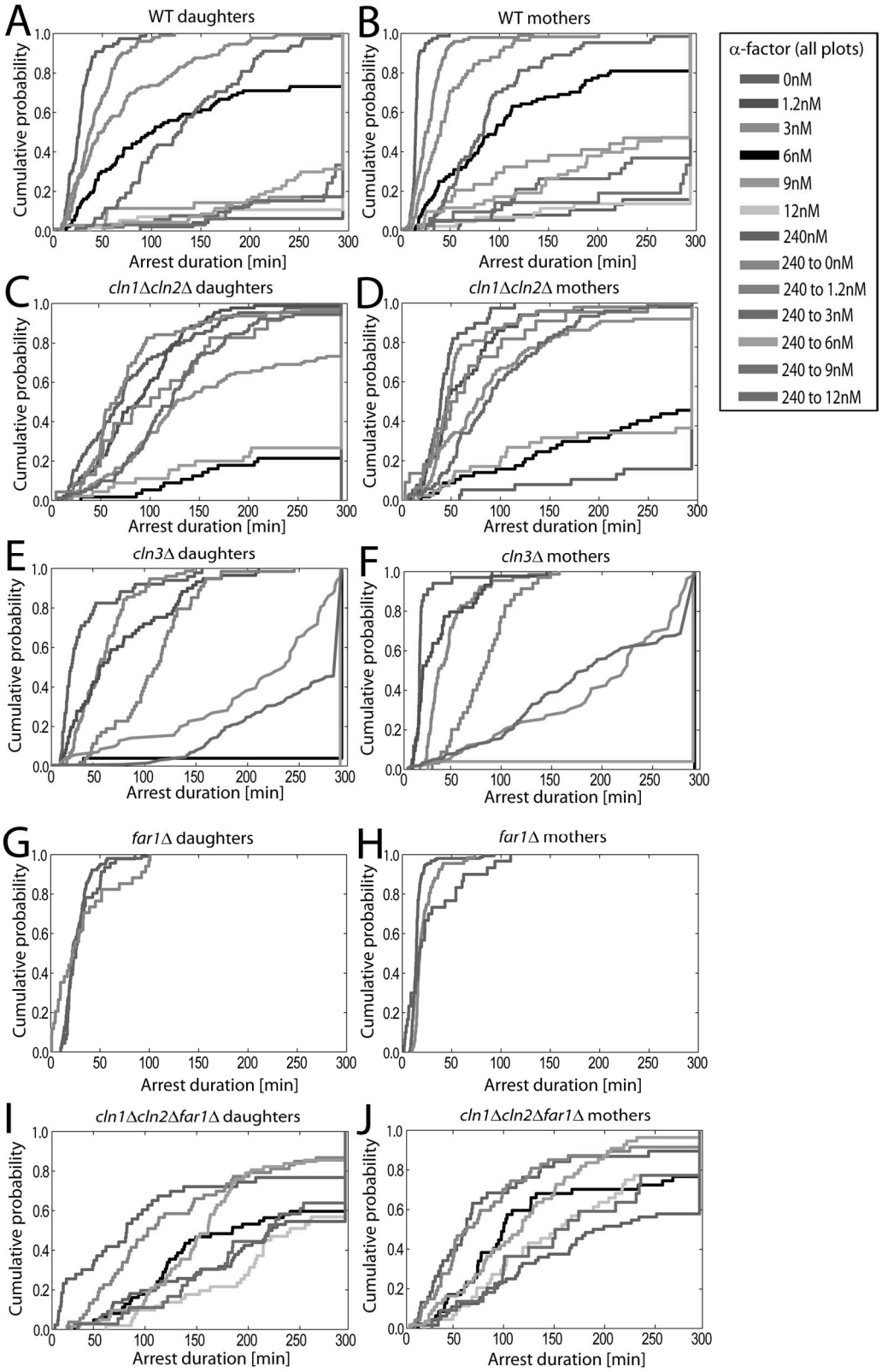

Cumulative probability distributions for Fig. 2 and S2 (A-J) Data here corresponds to results shown in Fig. 2B-D and Fig. S2, which show our estimates for the medians and their 95% confidence intervals. Note that the same color represents the same history of α-factor concentration in all sub-figures.

Figure S4, related to Figure 3:

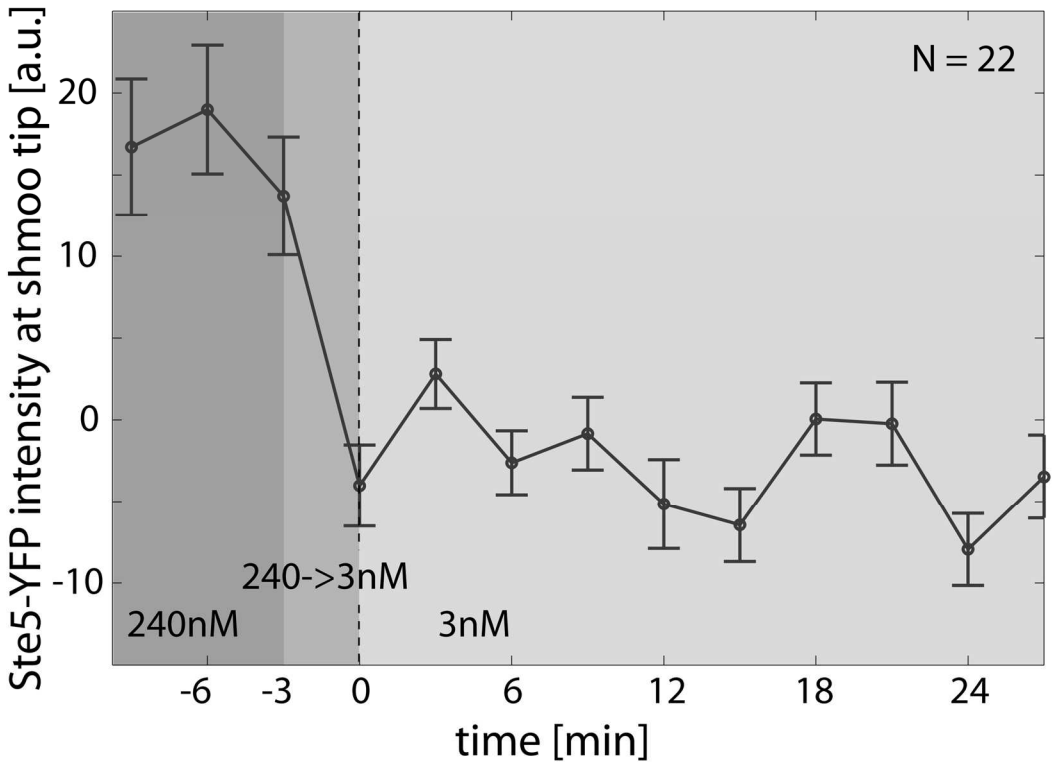

Ste5 responds rapidly to mating pheromone reduction: Cells containing an integrated *STE5-YFP* scaffold fusion protein were grown in synthetic complete media (SCD) after which they were exposed to a 30min pulse of 240nM α-factor followed by 3nM α-factor for 300min. Next, the cells were segmented and kymographs were created as in Fig. 3G,H,I. We here show the mean ± standard error of 22 kymographs at the time of pheromone downshift. We note a clear downshift between the last time point with 240nM α-factor ('time = -3') and the first with 3nM ('time = 0') suggesting that the shmoo-localized Ste5 responds in less than 3 minutes to changes in mating pheromone in support of our findings from Fig. 3A,B.

FigureS5, related to Figure 4:

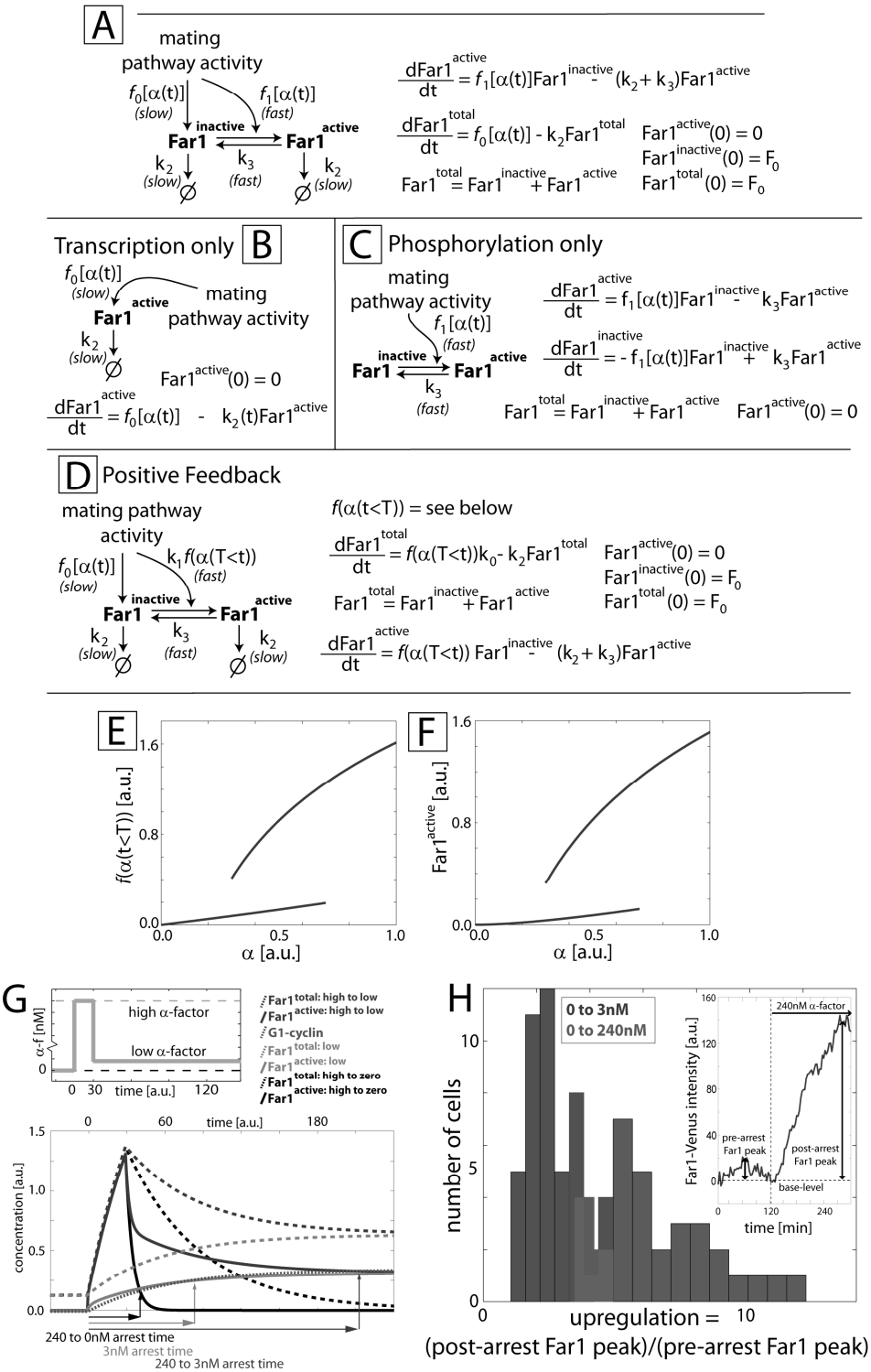

Far1 arrest performance for alternate regulatory mechanisms: (A-D) See text for more details. (E) Assumed form of the function representing MAPK activity f(α(t)) = -ln(1-0.25t) for t increasing < 0.7 and = 3+ln(0.25t) for t decreasing > 0.3. (F). Resulting hysteretic steady-state level of active Far1. (G) Extended analysis corresponding to Fig. 4B in the main text showing the response of three different treatments: high to low, high to zero and low only. This reflects the 240 to 3nM, 240 to 0nM and 3nM only experiments. Note that Far1 activity is countered by (i) A

rising concentration of G1 cyclins (magenta) as determined in Fig. 3E,F in the main text and (ii) Cellular dilution as shown in Fig. 4E,F in the main text (not included in this simple model). The dynamics of the G1-cyclins used here is based on an exponential fit of the data presented in Fig. 3F. For high concentrations of mating pheromone we assume that the steady state level of active Far1 is higher than the combined effect of G1-cyclins and dilution (cellular growth in impeded in shmooing cells), explaining how permanent arrest can be maintained. Conversely, cells in low concentrations of pheromone are assumed to stay arrested until the combined effects of dilution and G1-cyclin activity drives cell cycle reentry. (H) *Far1 is up-regulated ~6-fold during arrest*: To estimate the noise buffering capacities for the feed-forward system we calculated the relative pheromone induced upregulation of Far1. Cells were grown in SCD for 120min and then exposed to 240 (red) or 3nM (blue) of α-factor. Pre- and post-arrest Far1 peaks were compared for 32 and 47 cells (240nM and 3nM) and mean up-regulations (± standard deviation) of 6.6±2.2 and 2.6±1.0 -fold were found. See panel for example cell trace.

Figure S6, related to Figure 5:

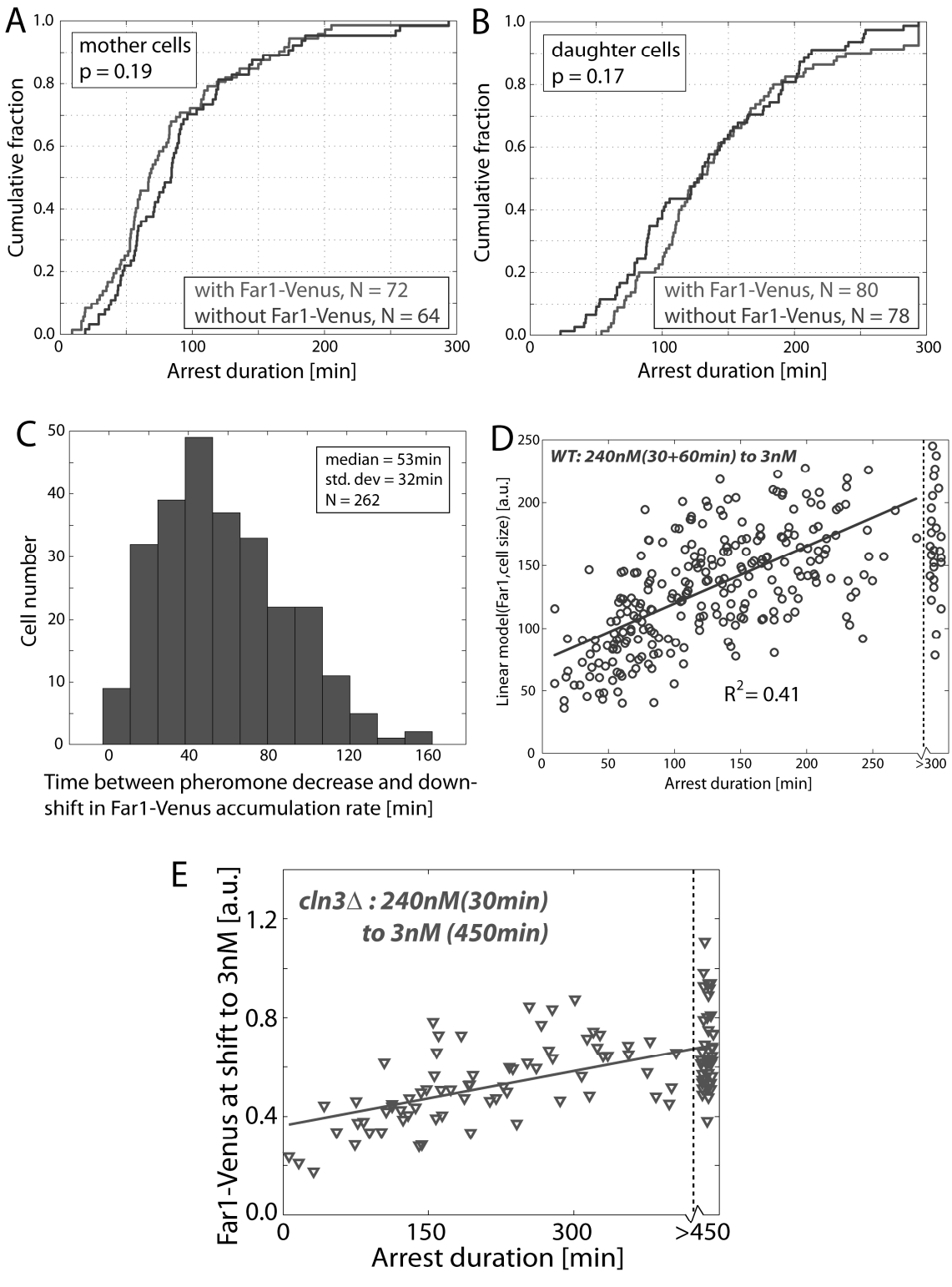

Effect of N-terminal Venus fusion and cell size on reentry analyzed: (A,B) Control for effect of C-terminal Far1-Venus fusion. Cells expressing C-terminal FAR1-Venus fusion from the endogenous locus exhibit identical arrest kinetics to WT cells. Mating arrest duration was measured for the hysteresis experiment (see Fig. 2A) using a 30 minute pulse of 240nM α-factor followed by 300 minutes of 3nM α-factor in cells with or without *Venus* fused to *FAR1*. No significant differences were observed between these genotypes for either mother (A) or daughter (B) cells. (C) *Time between pheromone decrease and decrease in Far1-Venus:* Distribution of times between decrease of pheromone and Far1 accumulation down-shift (cf red arrow Fig. 5C in main text). The delay between the measured downshift of Far1-Venus accumulation and the change in pheromone concentration is likely the result of Venus maturation kinetics (Charvin et al., 2008). (D) *Linear model of arrest duration(cell size, Far1).* The best linear model including peak Far1 level and cell size is duration [in minutes] = 158*Far1(peak level) − 0.12 * (cell area in pixels) -81. Including cell size to the fit improved the fit significantly ($p<1e-6$) whereas no significant improvement was found by including cell type ($p=0.43$). This suggests that no information about the cell type (mother/daughter) is retained after mating arrest, but that larger cells reenter the cell cycle more rapidly. This may be due to increases in Cln3 activity (Fig. 3E,F), which are known to be size dependent(Turner et al., 2012). (E) *Extended arrest of cln3Δ cells.* Since a large fraction of *cln3Δ* cells arrest longer than 300min (Fig. 3G), we repeated the experiment correlating Far1 levels with arrest duration and observed cells for a longer period of time. The repeated experiment allows observation of reentry up to 450 minutes rather than 300 minutes as shown in Fig. 5. Far1 amounts remains correlated with the arrest time; $R^2 = 0.40$.

Figure S7, related to Figure 6:

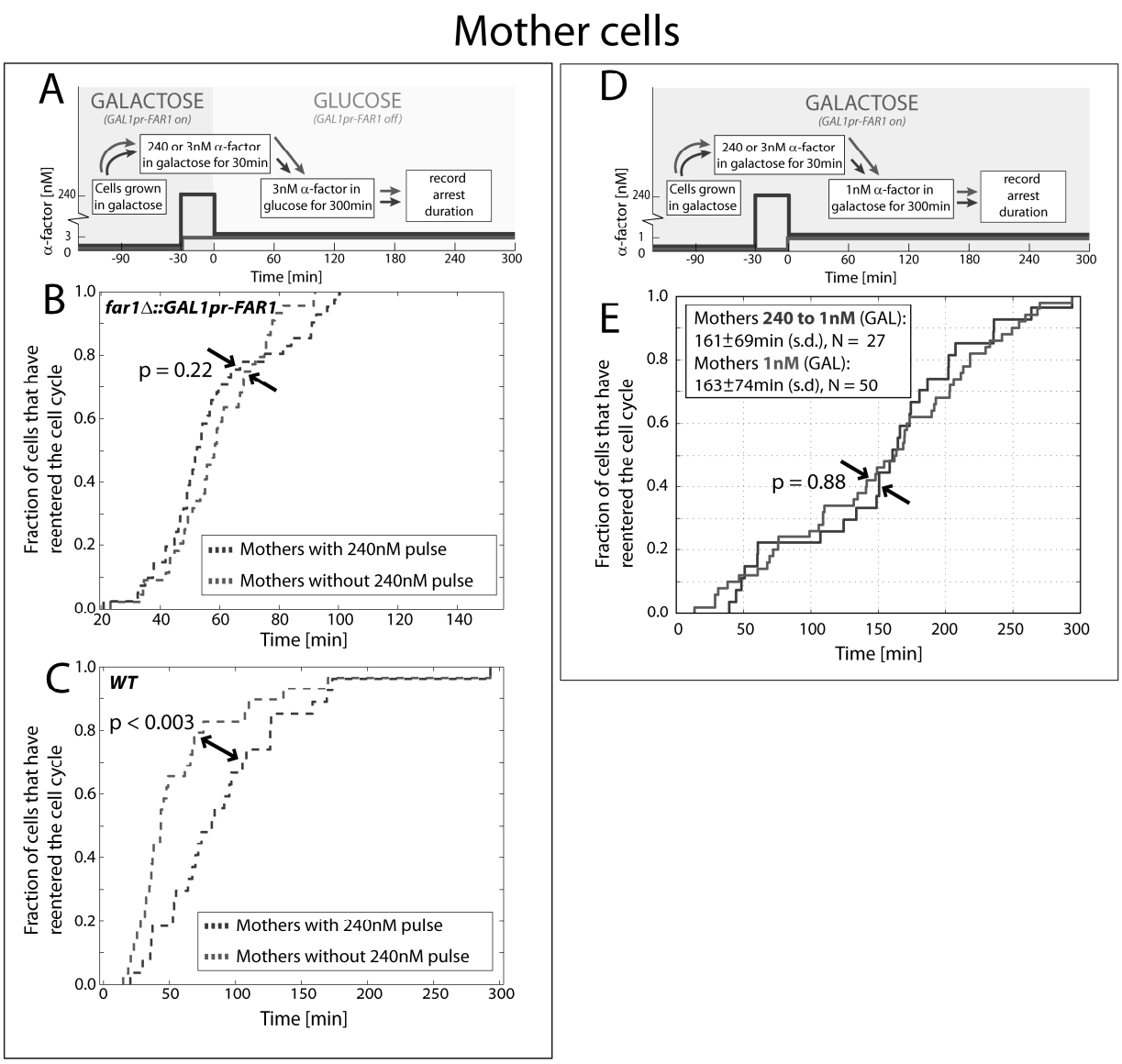

Exogenous control of FAR1 transcription eliminates hysteresis in mothers: (A-C) The corresponding data for daughter cells are shown in Fig. 6 in the main text. (A) Experiment schematic. (B,C) Arrest duration distributions are shown for mother cells expressing *FAR1* from the galactose inducible *GAL1* promoter and for WT control cells. (D,E) *Hysteresis eliminated by constitutive FAR1 expression.* No hysteresis was observed in cells with *GAL1pr-FAR1* grown in galactose for the duration of the experiment so that *FAR1* was continually expressed. To control for the possibility that the absence of hysteresis in Fig. 6 is a byproduct of turning off *FAR1* transcription, we repeated the hysteresis experiment from Fig. 6A,B but without shifting the cells to glucose (D). Cells were exposed to low (1nM) concentration of α-factor after the pulse. In these conditions the cells arrested for a long time (presumably due to the excess of Far1-protein) but no hysteresis was observed for daughter cells (Fig. 6E) and mother cells (E). This result supports our hypothesis that hysteresis arises solely from Far1 accumulation.

Figure S8, related to Figure 7:

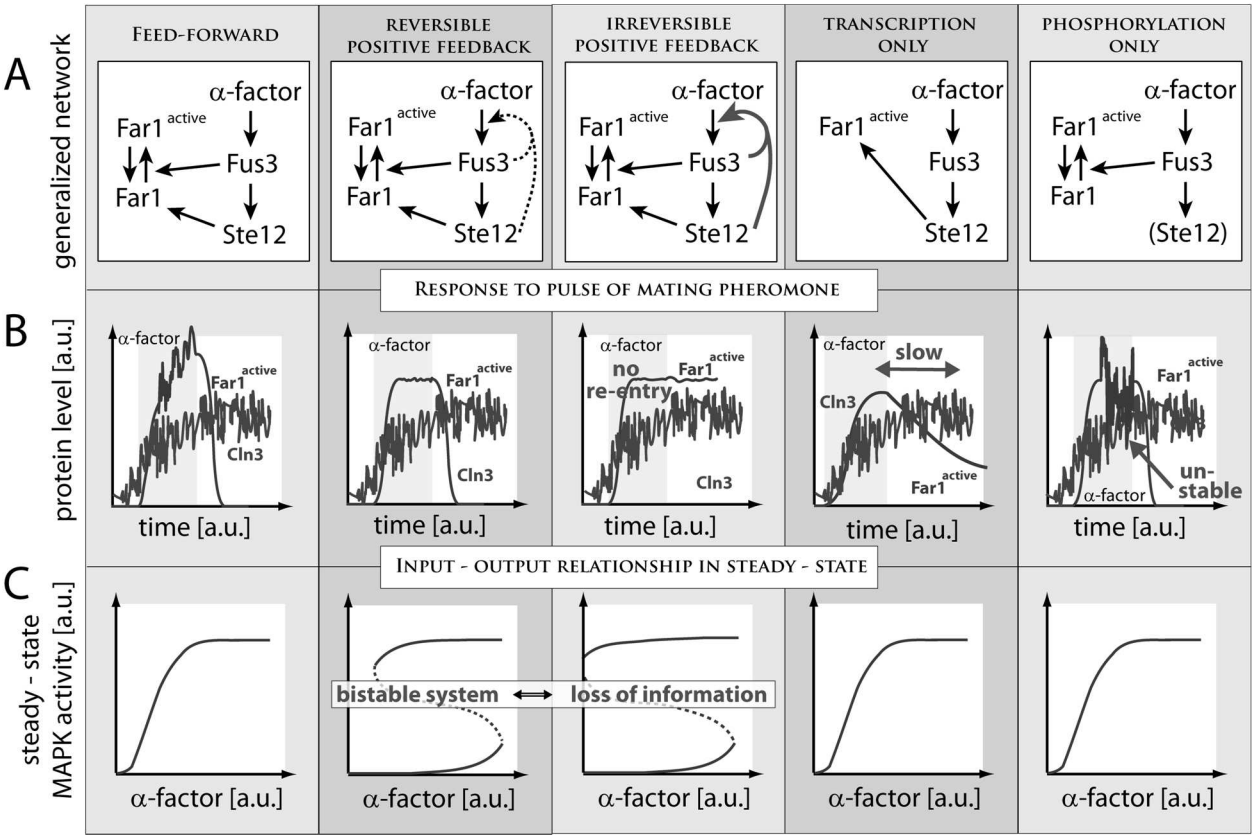

Alternative Far1 regulatory mechanisms are deficient: (A) We here consider five categories of networks controlling the level of active Far1. (B,C) We here show a general response for the networks to a square pulse of mating pheromone (B) and the steady state relationship between MAPK activity and mating pheromone (C). Only the feed-forward regulation fulfills all requirements (rapid activation and reentry, ability to continually sense extracellular information, and robustness to noise).

Table S1

Genotype	*Start 4xCLN2*	*Start* WT	*Start cln1Δcln2Δ*	Re-entry *4xCLN2*	Re-entry WT	Re-entry *cln1Δcln2Δ*	Re-entry *cln3Δ*	Re-entry *STE5-8A*	Re-entry *FAR1-S87A*	Re-entry *STE5-8A FAR1-S87A*	Re-entry *3xFAR1*
Start 4xCLN2	1	0.035	6.8e-7	0.26	4.5e-7	4.9e-7	5.9e-8	3.5e-12	1.0e-11	4.0e-15	6.4e-7
Start WT		1	2.8e-4	0.31	4.3e-5	7.1e-6	2.6e-6	1.3e-9	8.3e-10	1.1e-12	1.1e-4
Start cln1Δcln2Δ			1	1.5e-4	0.74	0.32	0.30	9.3e-3	5.1e-3	3.9e-4	0.61
Re-entry *4xCLN2*				1	6.0e-5	5.3e-5	6.6e-6	2.0e-9	1.6e-9	3.3e-12	4.9e-5
Re-entry WT					1	0.36	0.50	0.036	0.016	2.9e-3	0.91
Re-entry *cln1Δcln2Δ*						1	0.70	0.28	0.20	0.085	0.49
Re-entry *cln3Δ*							1	0.20	0.081	0.034	0.59
Re-entry *STE5-8A*								1	0.44	0.33	0.087
Re-entry *FAR1-S87A*									1	0.96	0.027
Re-entry *STE5-8A FAR1-S87A*										1	9.8e-3
Re-entry *3xFAR1*											1

Pairwise genetic analysis of forced cell cycle reentry (Fig. 1; Fig. S1): Arrested cells of the specified genotype were exposed to a pulse of exogenous Cln2 expressed from a *MET3* promoter as described in Fig.1 A-C and the methods. Also included are data for *Start* (the Whi5-GFP cell cycle commitment threshold in cycling cells exposed to a step increase in mating pheromone; see text and (Doncic et al., 2011)) for WT, *cln1*Δ*cln2*Δ and *4xCLN2* cells. Commitment data for both datasets was pooled and a model based solely on nuclear Whi5-GFP was constructed. A second variable, valued 0 for one genotype and 1 for the other, was then added. P-values for genotype influence were then calculated using a $\chi 2$ test implemented with the *add1* function in R. Blue shaded regions indicate p<1e-2

Table S2

Genotype	WT	WT (60min)	*cln1*Δ *cln2*Δ	*cln3*Δ	*clb5*Δ *clb6*Δ
WT	1	>0.05	>0.05	<0.01	<0.01
WT (60min)		1	>0.05	<0.01	<0.01
*cln1*Δ *cln2*Δ			1	<0.01	<0.01
*cln3*Δ				1	<0.01
*clb5*Δ *clb6*Δ					1

Pairwise comparison of linear models of arrest duration shown in Fig. 5: Statistical pair wise comparison of linear models for arrest duration as a function of Far1-Venus amount after the high-pheromone pulse for *WT*, *cln1*Δ*cln2*Δ, *cln3*Δ and *clb5*Δ*clb6*Δ cells. Data shown in Fig. 5D-I. Red indicates that the relationship between Far1-Venus and arrest duration is not significantly different between the two genotypes ($p>0.05$ as determined by a χ^2 test implemented in R using the add1 function).

Table S3

Parameter	value	Source
$f_1[\alpha(t)]$	1min^{-1}	AD, experimental estimate (unpublished)
k_2	0.01min^{-1}	Dilution/degradation calculation (Fig. 4E,F)
k_3	$0.1\ \text{min}^{-1}$	AD, experimental estimate (unpublished)

Parameters for numerical simulations: To compare the different models we calculate arrest, reentry and noise-resistance times using the following set of parameters. All parameter values used are as stated here unless otherwise indicated. The parameter values were estimates as follows: Time to arrest upon exposure to step increase in mating pheromone gives us $f_1[\alpha(t)]$, dilution/degradation (fig. 4E,F) gives us k_2. k_3 is estimated based on the time it takes for arrested cells to reenter the cell cycle upon complete mating pheromone removal.

Table S4

Protein	Data for asynchronous cells		Estimated peak abundance
	(Ghaemmaghami et al., 2003)	(Cross et al., 2002)	
Cln1	319	995 ± 231	~2000 (Post *Start*)
Cln2	1270	2011 ± 504	~4500 (Post *Start*)
Cln3	Not detected	216 ± 44	~500 (late M)
Far1	238	NA	~5000 (pheromone arrest)

Estimation of protein numbers: We here assume that Cln1 and Cln2 follows similar dynamics and that they are expressed during ~33% of the cell cycle and absent otherwise (Bean et al., 2006). Cln3 fluctuates weakly during the cell cycle and we estimated its peak abundance based on data in (Tyers et al., 1993) combined with the data for asynchronous cells from (Cross et al., 2002). For Far1, we take advantage of the fact that Far1 is only expressed during G1(McKinney et al., 1993), ~20% of the total cell cycle time (Fig. S3) and absent otherwise to estimate a peak value for cycling cells (~1000). This number is further upreguated ~5 times upon pheromone stimulation (see Fig. S5H and (Chang and Herskowitz, 1990)) giving us the final number.

Table S5

Name	Genotype	Source
JS136-3c	*MATa bar1::URA3 trp1::TRP1-MET3pr-CLN2 WHI5-GFP-kanMX HTB2-mCherry-spHIS5*	(Doncic et al., 2011)
JS146-8c	*MATa bar1::URA3 cln1::HIS3 cln2⊿ trp1::TRP1-MET3pr-CLN2 WHI5-GFP-kanMX HTB2-mCherry-spHIS5*	(Doncic et al., 2011)
JS150-5b	*MATa bar1Δ STE5-8A trp1::TRP1-MET3pr.-CLN2 WHI5-GFP-kanMX HTB2-mCherry-spHIS5*	(Doncic et al., 2011)
JS151-6	*MATa bar1::URA3 far1:kanMX trp1::TRP1-MET3pr-CLN2 WHI5-GFP-kanMX*	This study
JS187-1	*MATa bar1::URA3 FAR1-S87A STE5-8A trp1::TRP1-MET3pr-CLN2 WHI5-GFP-kanMX HTB2-mCherry-spHIS5*	(Doncic et al., 2011)
JS193-5c	*MATa bar1⊿ 3XCLN2pr-mCherry-PEST-NLS ura3::URA3-FUS1pr-GFP-NLS*	(Doncic et al., 2011)
JS196-4	*MATa bar1Δ CLN2::3xCLN2-URA3 trp1::TRP1-MET3pr-CLN2 WHI5-GFP-kanMX HTB2-mCherry-spHIS5*	(Doncic et al., 2011)
JS197-29b	*MATa bar1Δ bar1::URA3 trp1::TRP1-MET3pr-CLN2 WHI5-GFP-kanMX HTB2-mCherry-spHIS5 cln3::LEU2 ADE2*	(Doncic et al., 2011)
JS211-5b	*MATa bar1::URA3 FAR1-S87A trp1::TRP1-MET3pr-CLN2 WHI5-GFP-kanMX HTB2-mCherry-spHIS5*	(Doncic et al., 2011)
JS217-2b	*MATa bar1⊿ cln1::HIS3 cln2⊿ trp1::TRP1-MET3pr-CLN2 WHI5-GFP-kanMX HTB2-mCherry-spHIS5 far1::cglaLEU2*	This study
JS221-4	*MATa FAR1-Venus-kanMX WHI5-mCherry-spHIS5*	(Doncic et al., 2011)
JS264-6c	*MATα bar1::URA3 cln1::HIS3 cln2⊿ cln3⊿::LEU2 ADE2 trp1::TRP1-MET3pr-CLN2 FAR1-Venus-kanMX WHI5-mCherry-spHIS5*	This study
AD2-8c	*MATa bar1::URA3 trp1::TRP1-MET3pr-CLN2 WHI5-mCherry-spHIS5 FAR1-Venus-kanMX ADE2*	This study
AD4-43d	*MATa bar1::URA3 cln3::LEU2 WHI5-mCherry-spHIS5 FAR1-Venus-kanMX ADE2*	This study
AD5-17d	*MATa bar1::URA3 trp1::TRP1-MET3pr-CLN2 WHI5-mCherry-spHIS5 FAR1-Venus-kanMX ADE2 cln1::HIS3 cln2⊿*	This study
AD18-5	*MATa bar1::URA3 WHI5-mCherry-spHIS5, ADE2, far1⊿::TRP1-GAL1pr-FAR1-Venus-kanMX*	This study
AD19-36d	*w303a bar1::Nat Whi5-mCherry-SpHIS5 ADE2 Far1-Venus-KMX trp::TRP-MET3pr-CLN2 clb5::URA3 clb6::LEU2*	This study
TCY3057	*MATa bar1Δ ste5::STE5-YFP trp1::STE5pr-YFP-STE5-TRP1*	(Yu et al., 2008)

List of strains: All strains were obtained by standard methods, are congenic with W303 (leu2-3,112 his3-11,15 ura3-1 trp1-1 can1-1), and were constructed from laboratory stocks.

Supporting references

Bean, J.M., Siggia, E.D., and Cross, F.R. (2006). Coherence and timing of cell cycle start examined at single-cell resolution. Mol Cell *21*, 3-14.

Busti, S., Gotti, L., Balestrieri, C., Querin, L., Drovandi, G., Felici, G., Mavelli, G., Bertolazzi, P., Alberghina, L., and Vanoni, M. (2012). Overexpression of Far1, a cyclin-dependent kinase inhibitor, induces a large transcriptional reprogramming in which RNA synthesis senses Far1 in a Sfp1-mediated way. Biotechnol Adv *30*, 185-201.

Chang, F., and Herskowitz, I. (1990). Identification of a gene necessary for cell cycle arrest by a negative growth factor of yeast: FAR1 is an inhibitor of a G1 cyclin, CLN2. Cell *63*, 999-1011.

Charvin, G., Cross, F.R., and Siggia, E.D. (2008). A microfluidic device for temporally controlled gene expression and long-term fluorescent imaging in unperturbed dividing yeast cells. PLoS ONE *3*, e1468.

Cross, F.R., Archambault, V., Miller, M., and Klovstad, M. (2002). Testing a mathematical model of the yeast cell cycle. Mol Biol Cell *13*, 52-70.

Doncic, A., Falleur-Fettig, M., and Skotheim, J.M. (2011). Distinct interactions select and maintain a specific cell fate. Mol Cell *43*, 528-539.

Ghaemmaghami, S., Huh, W.K., Bower, K., Howson, R.W., Belle, A., Dephoure, N., O'Shea, E.K., and Weissman, J.S. (2003). Global analysis of protein expression in yeast. Nature *425*, 737-741.

McKinney, J.D., Chang, F., Heintz, N., and Cross, F.R. (1993). Negative regulation of FAR1 at the Start of the yeast cell cycle. Genes Dev *7*, 833-843.

Turner, J.J., Ewald, J.C., and Skotheim, J.M. (2012). Cell size control in yeast. Curr Biol *22*, R350-359.

Tyers, M., Tokiwa, G., and Futcher, B. (1993). Comparison of the Saccharomyces cerevisiae G1 cyclins: Cln3 may be an upstream activator of Cln1, Cln2 and other cyclins. Embo J *12*, 1955-1968.

Yu, R.C., Pesce, C.G., Colman-Lerner, A., Lok, L., Pincus, D., Serra, E., Holl, M., Benjamin, K., Gordon, A., and Brent, R. (2008). Negative feedback that improves information transmission in yeast signalling. Nature *456*, 755-761.